Check for updates

RESEARCH ARTICLE

REVISED Nanoparticles as microstructure architects: A phase-field study on electrodeposited coatings

[version 2; peer review: 2 approved with reservations]

Javier Fernández Troncoso, Christian Eike Precker, Andrea Gregores Coto, Santiago Muíños Landín

AIMEN Centro Tecnologico, O Porriño, Galicia, Spain

v2 **First published:** 07 Sep 2026, **6**:327
https://doi.org/10.12688/openreseurope.24692.1

Latest published: 15 Oct 2026, **6**:327
https://doi.org/10.12688/openreseurope.24692.2

Abstract

The electrodeposition of polycrystalline nickel coatings with tailored microstructures is critical for enhancing mechanical performance and surface quality. However, while experimental studies show that nanoparticles can refine grains and prevent columnar growth, it is still not clear what nanoparticle types, concentrations and shapes minimize this phenomenon. In this work, we combine phase-field modelling and a machine learning approach to study the impact of material and process parameters on the resulting microstructures during electrodeposition. We simulated polycrystalline nickel electrodeposition in the presence of nanoparticles with varying geometries (spherical and 2D) and concentrations, and used Random Forest classifier, interpreted via Shapley additive explanation analysis, to identify the key parameters controlling microstructural evolution. Our results quantitatively demonstrate that the gradient coefficient and overpotential are the most influential factors, while nanoparticle concentration and shape are critical in suppressing columnar growth. Specifically, we observed that 2D nanomaterials like MoS2 or graphene are of high interest when their volume fraction is larger than 3% since they reduce drag and promote smooth interface movement, thus preventing columnar growth.

Keywords

electrodeposition, phase-field, digital twins, computational modeling, artificial intelligence

Open Peer Review

Approval Status ? ?

	1	2
version 2 (revision) 15 Oct 2026		
version 1 07 Sep 2026	? view	? view

1. **Michael A Pence**, The University of Utah, Salt Lake City, USA

2. **Suresh Velayudham**, Sona College of Technology, Salem, India

Any reports and responses or comments on the article can be found at the end of the article.

HE This article is included in the Horizon Europe gateway.

Corresponding author: Javier Fernández Troncoso (javier.fernandez@aimen.es)

Author roles: Fernández Troncoso J: Conceptualization, Data Curation, Investigation, Methodology, Resources, Software, Visualization, Writing – Original Draft Preparation; **Precker CE**: Conceptualization, Project Administration, Validation, Writing – Review & Editing; **Gregores Coto A**: Validation, Writing – Review & Editing; **Muíños Landín S**: Conceptualization, Funding Acquisition, Project Administration, Supervision, Writing – Review & Editing

Competing interests: No competing interests were disclosed.

Grant information: This project has received funding from the European Union's Horizon Europe research and innovation programme under grant agreement No. 101058450 (MOZART).
The funders had no role in study design, data collection and analysis, decision to publish, or preparation of the manuscript.

Copyright: © 2026 Fernández Troncoso J *et al*. This is an open access article distributed under the terms of the Creative Commons Attribution License, which permits unrestricted use, distribution, and reproduction in any medium, provided the original work is properly cited.

How to cite this article: Fernández Troncoso J, Precker CE, Gregores Coto A and Muíños Landín S. **Nanoparticles as microstructure architects: A phase-field study on electrodeposited coatings [version 2; peer review: 2 approved with reservations]** Open Research Europe 2026, **6**:327 https://doi.org/10.12688/openreseurope.24692.2

First published: 07 Sep 2026, **6**:327 https://doi.org/10.12688/openreseurope.24692.1

REVISED **Amendments from Version 1**

In this second version, the reviewer's comments have been addressed. The text is more detailed and complete, and more Figures (3,4,5) and Table (2) have been incorporated.

Any further responses from the reviewers can be found at the end of the article

1. Introduction

Nanostructured coatings are a cornerstone of advanced surface engineering, offering superior mechanical strength, enhanced wear resistance and improved functional properties compared to conventional microcrystalline materials.[1] The performance of these coatings is intrinsically governed by a complex interplay of material composition, microstructure and processing parameters and the choice of the right manufacturing process is critical to generate reliable, safe and durable structures. Among the various fabrication techniques, electrodeposition has emerged as a particularly versatile and scalable method for producing dense and porosity-free nanocrystalline coatings. Electrodeposition is a process in which a metal or alloy is deposited onto a conductive substrate in the presence of an electric current and is commonly used for coating materials by enhancing their surface properties, including corrosion and wear resistance or electrical conductivity. The process involves immersing the substrate (cathode) and a metal source (anode) in an electrolyte solution (bath) containing metal ions. When an external voltage is applied, metal ions migrate towards the cathode and reduce to form a thin, uniform metal coating. Within this field, nickel (Ni) electrodeposition is of paramount industrial importance due to the material's excellent corrosion resistance, hardness and ability to form uniform coatings,[2] which makes it one of the most employed metals for both functional and decorative purposes, with multiple applications in different industries, including electronics, automotive and aerospace.[2] When voltage is applied, metal ions undergo reduction at the cathode, forming a solid metal deposit through the reaction $^{Ni^{2+}} + 2e^{-} \rightarrow Ni$ during Ni deposition.

During electrodeposition, several main components dispersed in the bath guarantee coating stability and quality, including metal salts, additives, acids and nanoparticles (NPs). Metal salts serve as the source of metal ions, ensuring a steady supply of ions for deposition. Additives play a crucial role in modifying the deposit characteristics, including leveling agents for surface smoothness, brighteners for enhanced reflectivity, suppressors for controlled deposition rates and stress relievers to prevent internal defects like cracking or peeling. Acids, such as sulfuric acid (H_2SO_4) and boric acid (H_3BO_3), regulate pH and conductivity, ensuring stable electrochemical reactions.[3] NPs can be incorporated into the bath to form composite coatings, improving hardness and corrosion resistance. Frequently, surfactants are also present to prevent aggregation and segregation phenomena.

The presence of NPs in the bath results in an enhancement of the corrosion resistance, since they can act as physical barriers against corrosive agents.[4] Additionally, they can also reduce friction by facilitating easy shear between layers and improve wear resistance by reinforcing the metal matrix against mechanical degradation.[5] Therefore, the study of the impact of NPs on surface texture is critical. The incorporation of NPs into the Ni polycrystalline matrix during electrodeposition significantly influences the solidification process, affecting both columnar growth and surface texture, since they can act as heterogeneous nucleation sites, promoting the formation of finer grains and altering the crystallographic texture of the deposit.[6] In particular, second-phase hard ceramic particles, such as alumina (Al_2O_3), magnesia (MgO) and silicon carbide (SiC) have been widely incorporated into nickel matrices to enhance the mechanical, tribological and high-temperature performance of electrodeposited coatings. During co-deposition, these inert ceramic micro/nanoparticles act as physical barriers by restricting local Ni^{2+} diffusion flux, resulting in kinetic and mass transport obstruction, and interrupting grain growth via interfacial pinning. Spherical ceramic geometries (Al_2O_3, SiC) act as localized discrete pinning sites that disrupt long-range columnar order, promoting grain refinement and transitions toward equiaxed growth, In contrast, 2D nanomaterials such as graphene and MoS_2 possess unique planar geometries, exceptionally high aspect ratios and superior intrinsic mechanical and tribological properties that lead to anisotropic spatial orientation during codeposition, acting as extensive physical barriers to metal ion transport and interface movement. Graphene provides mechanical reinforcement and high electrical conductivity, while MoS_2 offers exceptionally low shear strength and friction coefficients due to its weak interlayer van der Waals bonding. Incorporating these 2D materials into Ni electrodeposits could act as low-drag obstacles and suppress columnar grain growth compared to conventional 0D/3D spherical particles. Therefore, the NP concentration, size and shape play crucial roles in these effects. Higher concentrations of NPs generally increase the number of nucleation sites, resulting in a more pronounced grain refinement. However, excessive NP content can lead to agglomeration, which may adversely affect the uniformity of the deposit. Similarly, smaller particles provide a larger surface area for nucleation but may be more prone to agglomeration, and the shape of the NPs influences their interaction with the growing matrix and can promote anisotropic growth. This would prevent columnar growth, thus enhancing mechanical properties, since columnar grain boundaries facilitate crack

propagation. Furthermore, NPs also promote the formation of smoother and more compact surfaces.[4] Additionally, as well as the chemical composition, properties of electrodeposited Ni like texture or hardness are highly sensitive to process parameters. These include the bath temperature, current density and the use of agitation methods.

Due to the importance of NPs and fabrication process parameters during electrodeposition, different experimental techniques and simulation methods have been employed for this analysis in the literature. Experimentally, coatings generated in the presence of NPs have been characterized using scanning electron microscopy (SEM), transmission electron microscopy (TEM), X-ray diffraction (XRD) and energy-dispersive X-ray spectroscopy (EDS) to analyze microstructure, NP distribution and phase composition. Mechanical and corrosion properties have been evaluated via hardness tests, wear tests and electrochemical measurements.[4,6–9] Simulation methods, such as molecular dynamics (MD), finite element analysis (FEA) and Monte Carlo simulations, have been used to model NP-matrix interactions, deposition kinetics and stress distribution, providing insight into the mechanisms governing NP incorporation and coating performance.[10–13] However, it was still not possible to understand the impact of NP properties together with process parameters on final coating properties. To address this gap, we developed a phase-field model to simulate the polycrystalline electrodeposition of nickel in the presence of NPs with varying geometries and concentrations. The insights from these simulations are then analyzed using machine learning (ML), specifically a Random Forest classifier, to identify the most influential parameters controlling microstructure development. Furthermore, Explainable Artificial Intelligence (xAI) techniques, namely the SHAP tree explainer, are applied to decode the complex, non-linear relationships within the model. This combined methodology aims to provide a deeper, more fundamental understanding of the electrodeposition process, offering predictive capabilities that can guide the experimental design of next-generation nanocomposite coatings. The simulation methodology and ML framework are detailed in Section 2, with the results and discussion presented in Section 3.

2. Methods

a. Phase-field modelling

Phase-field modelling is a computational technique that uses continuous field variables to describe microstructural evolution by solving coupled partial differential equations based on thermodynamic and kinetic principles.[14–16] In the study of the polycrystalline Ni electrodeposition with NPs suspended in the electrolyte, we characterize the different Ni grains with order parameters ε_i where $i = 1 \ldots N$ and N is the number of grains, and the different NPs with order parameters ϵ_j where $j = 1 \ldots M$ and M is the number of NPs. These order parameters take the value 1 inside the region they represent and 0 outside, and all of them are equal to 0 in the electrolyte. Additionally, the concentration of ions in the electrolyte is described by the concentration field c and the electrostatic potential field by the variable ϕ. The general equations governing the evolution of the order parameters and concentration are given by the Allen-Cahn and Cahn-Hilliard equations,[17] respectively:

$$\frac{\partial \epsilon_i}{\partial t} = -L\frac{\delta G}{\delta \epsilon_i},$$

$$\frac{\partial c}{\partial t} = \nabla M \nabla \frac{\delta G}{\delta c},$$

where L is the interface mobility, M is the ion mobility and G is the total free energy of the system. Since the total free energy includes chemical, gradient and electrostatic contributions, the equations for the evolution of the order parameters representing Ni grains can be written as[18]:

$$\frac{\partial \varepsilon_i}{\partial t} = -L_\sigma\left(g'(\varepsilon_i) - \kappa\nabla^2\varepsilon_i - \gamma_{\text{nuc}}h'(\varepsilon_i)\sum\nolimits_j \epsilon_j\right)$$
$$-L_\eta h'(\varepsilon_i)\left[exp\left(\frac{(1-\alpha)nF\eta}{RT}\right) - cexp\left(\frac{-\alpha nF\eta}{RT}\right)\right] - \gamma_{\text{pin}}\vee\nabla\varepsilon_i\vee\sum\nolimits_j \epsilon_j,$$

where L_σ and L_η are the interface mobility and a pre-factor related to reaction exchange current, respectively, $g(\varepsilon) = W\varepsilon^2(1-\varepsilon)^2$ is a double well potential function with W being the transition barrier energy, which is different for the grain/liquid interface and grain/grain interface, $h(\varepsilon) = \varepsilon^3(6\varepsilon^2 - 15\varepsilon + 10)$ is an interpolation function, γ_{nuc} and γ_{pin} define the strength of the nucleation and pinning terms, κ is a gradient coefficient penalizing gradients, $\alpha = 0.5$ is a symmetric function, n is the cation valence, η is the overpotential, and R, T and F are the gas constant, room temperature and Faraday constant, respectively. Since no coarsening is observed during electrodeposition, the barrier energy is set to a larger value at grain/grain interfaces than at the Ni/electrolyte interface ($W_{\text{Ni-Ni}} = 10^5 W_{\text{Ni-liquid}}$, with $W_{Ni-\text{liquid}} = 7 \times 10^6 \text{J/m}^3$).[18] The overpotential η represents the excess potential energy due to the application of an external electrostatic field, and determines the reaction rate during electrodeposition. The second term, in brackets, represents the Butler-Volmer equation,[18] which controls the electrodeposition reaction rate.

On the other way, since NPs are considered as fixed particles and are not allowed to seggregate or aggregate, their positions do not change over time:

$$\frac{\partial \epsilon_j}{\partial t} = 0.$$

In this work, out-of-plane effects, particle rotation, aggregation and segregation are not captured. However, the assumption that NPs remain immobile and do not aggregate during the deposition process is supported by experimental observations under the operating conditions considered in this work.[19] In electrodeposition systems, NPs are typically stabilized in the electrolyte through a combination of Brownian motion, hydrodynamic agitation and the use of surfactants, which effectively prevent rapid aggregation and sedimentation.[19–21]

The evolution of the ion concentration is given by[18]:

$$\frac{\partial c}{\partial t} = \nabla \cdot \left(D\left(1 - \gamma_{NP} \sum\nolimits_j \epsilon_j\right) \nabla c \right) + \frac{Dc}{RT} nF \nabla \phi - \frac{c_s}{c_0} \sum\nolimits_i \frac{\partial \varepsilon_i}{\partial t},$$

where γ_{NP} determines how much NPs reduce the ion mobility, D is the ion diffusion coefficient, c_s is the site density of the metal and c_0 is the cation concentration in electrolyte. The last term represents the conversion of Ni^{2+} ions into Ni metal at the solid/liquid interface.

Finally, the electrostatic field evolves as follows[18]:

$$\nabla \cdot \left(\left(\sigma_e \left(1 - \sum\nolimits_i h(\varepsilon_i)\right) + \sigma_{\mathrm{Ni}} \sum\nolimits_i h(\varepsilon_i) \right) - \gamma_{NP}^{\sigma} \sum\nolimits_j \epsilon_j \right) \nabla \phi \Big) = +nFc_s \sum\nolimits_i \frac{\partial \varepsilon_i}{\partial t},$$

where σ_e and σ_{Ni} are the conductivities of the electrolyte and Ni phases, respectively, and γ_{NP}^{σ} quantifies the effect of the NPs on it.

The electrodeposition process was modeled using the described phase-field framework implemented via a custom Python script within the FEniCS finite-element library.[22,23] The simulations were performed on a 2D computational domain, where the coupled partial differential equations were solved to capture the evolution of the electrolyte/metal interface. Nanoparticles of specified geometries (spherical and 2D lamellar) and volume fractions were explicitly incorporated into the domain as immobile inclusions. Circular inclusions correspond to 2D projections of spherical NPs, whereas elongated rectangular inclusions represent lamellar particles, serving as simplified projections of plate-like nanomaterials such as graphene or MoS_2. These representations are not intended to reproduce the full three-dimensional morphology of NPs, but rather to capture their effective geometrical interaction with the evolving solid-liquid interface within a reduced-dimensional framework. However, since the key physical effects of interest, such as interfacial pinning, drag or anisotropic obstruction of grain growth, primarily depend on the local geometry and spatial distribution of obstacles relative to the growth direction, our consistent 2D framework allows evaluating the relative influence of NP geometry on microstructure evolution within our studied parameter space. Multiple simulations varying model parameters and NP concentrations and types were run to generate a database with details about 5789 phase-field simulations.

A numerical convergence study was performed to ensure the robustness of the simulation results. Mesh refinement analyses were conducted by systematically increasing the spatial resolution until variations in grain morphology, dynamics and stability became negligible. Similarly, time-step sensitivity was evaluated by reducing it and verifying that the evolution of the microstructure remained unchanged. These analyses confirm that the reported results are independent of the chosen discretization. Then, multiple simulations varying model parameters and NP concentrations and types were run to generate a database with details about 5789 phase-field simulations.

b. Artificial intelligence

i. Random Forest Classifier

The random forest classifier is an ML method used for classification tasks, which works by constructing multiple decision trees trained on different subsets of training data and returning the most common output as the final result. The algorithm begins by creating a diverse set of decision trees, each trained on a different subset of the training data. For each decision tree, the algorithm usually also selects a random subset of input features at each split point, rather than considering all features, which helps introduce variability among the trees and reduce the risk of overfitting. Thanks to their training algorithm, random forest classifiers are less sensitive to noise and outliers in the data, which makes them a powerful and

versatile algorithm that is widely used in various use cases, including text classification, image characterization or fraud detection.[24]

To ensure reproducibility and deterministic results, all random processes involved in data splitting and model training were controlled using fixed random seeds. The dataset was divided into training and test subsets using a fixed split, and the Random Forest model was initialized with the same seed. Input features were standardized using a scaling procedure to ensure comparable magnitudes, by removing the mean and scaling to unit variance to all features, and no feature selection was applied, as all variables correspond to physically meaningful model parameters. To verify robustness, the training and evaluation procedure was repeated across multiple data splits, yielding consistent performance and confirming that the results are not sensitive to a particular partition. Only input parameters were used as predictors, and no information derived from simulation outcomes was included in the feature set. The test dataset was strictly held during training, the entire dataset was found to be sufficiently balanced and model performance was verified across classes to ensure unbiased predictions by computing metrics such as precision, recall and F1-score.

In our study of the NP-reinforced electrodeposition process, the dataset comprised microstructural outcomes from 4497 phase-field simulations with spherical NPs and 1292 simulations with spherical 2D NPs projected in a 2D simulation box, and was randomly split into training (85%) and test (15%) datasets. We employed random forest classifier implemented via the scikit-learn Python module, utilizing an ensemble of 100 decision trees with Gini impurity as the splitting criterion. The classifier was trained to differentiate stable/unstable simulations, and then, for the stable ones, simulations with columnar or non-columnar growth. For both cases, the model's performance yielded an accuracy of 98.2% and 91.1%, respectively, and a macro-averaged F1-score of 0.97 and 0.88, respectively. A confusion matrix analysis confirmed high predictive accuracy in both classification problems with reduced small values in off-diagonal cells and consequently no significant bias. We observed a higher precision in the detection of non-columnar growth (0.91 vs 0.78 for non-columnar growth), thus meaning that it might be easier to apply reverse engineering via optimization algorithms when the target structures presented columnar growth. The use of random forest as classifiers is justified in Table 1, which provides a comparative benchmark study evaluating random forest, XGBoost, Support Vector Machine (SVM), k-Nearest Neighbors (k-NN) and Multi-Layer Perceptron (MLP). While the accuracy for the XGBoost, the random forest is the best model for predicting unstable simulations (higher precision), thus minimizing false-alarm classifications of valid simulation setups. Additionally, we conducted a systematic hyperparameter grid search evaluation to tune the key random forest parameters: the number of estimators and the maximum tree depth. Specifically, we evaluated candidate model configurations evaluating across numbers of estimators from 25 to 475 in increments of 25 and depth bounds including unconstrained depth and depths from 1 to 46 in steps of 5.

The trained random forest models were finally interpreted using SHAP (SHapley Additive exPlanations) to provide consistent, global feature importance rankings and individual prediction explanations. The details of this technique are provided in the following subsection.

ii. SHAP Tree Explainer

The SHAP Tree Explainer is a powerful xAI method for interpreting tree-based ML models, such as decision trees, random forests and gradient boosting models. In practical applications, SHAP Tree Explainer has been widely used in domains requiring xAI, including credit scoring, medical diagnosis and risk assessment.[25] It has proven to be a reliable tool for ensuring transparency in ML models, detecting biases, and uncovering unexpected model behaviours. It leverages game-theoretic principles to understand how different input variables impact the output of complex ensemble

Table 1. Comparative benchmark study evaluating different classification techniques in the prediction of unstable simulations.

Model	Accuracy [%]	Precision [%]		Recall [%]		F1-score	
		Unstable	Stable	Unstable	Stable	Unstable	Stable
Random forest	98.2	96	99	97	99	0.96	0.99
XGBoost	98.2	94	99	98	98	0.96	0.99
SVM	91.6	81	95	84	94	0.82	0.95
k-NN	86.6	72	91	68	92	0.70	0.91
MLP	94.2	85	97	91	95	0.88	0.96

models. The SHAP Tree Explainer works by decomposing a model's predictions into additive contributions from each feature, and the SHAP value for a feature is the average change in model output by conditioning on that feature when introducing features one at a time over all feature orderings.[26] The feature importance values reported in this work correspond to the mean absolute SHAP values computed across the samples in the dataset. This metric represents the average magnitude of the contribution of each feature to the model predictions and is used to rank the relative importance of the input parameters.

3. Results and Discussion

In this work, we simulated Ni electrodeposition in the presence of NPs with different types, shapes and sizes, at room temperature. The metal matrix consisted of polycrystalline Ni, with typical grain sizes around 10 μm, as observed experimentally with sizes between 1–10 μm depending on the type of current (direct or pulse) used, the current density, electrolyte composition, additives and bath temperature. Grain boundaries in electroplated Ni are generally stable during the plating process, meaning that grain growth during the electrodeposition process does not occur or is negligible. The number of NPs in the simulation domain and their radius influences the effective interaction with grain boundaries. Larger particles provide stronger pinning effects due to their increased interfacial contact, whereas smaller particles contribute to a more homogeneous distribution of pinning sites. However, the NP sizes and fractions used in the present work are in good agreement with the observed in experiments, where NPs sizes are comparable or slightly smaller than the initial Ni grain sizes.[27–29] Additionally, experiments showed that NPs do not have a driving force to move towards the solid/liquid interface without the influence of an external field, and they do not immediately segregate, precipitate or accumulate at this interface. NPs remain suspended in the bath, maintained by Brownian motion and agitation within the electrolyte. Surfactants are also often used to stabilize the NPs and prevent agglomeration, thus contributing to a uniform distribution of NP sizes throughout the electrolyte.[19]

During electrodeposition, it was observed that solidification and deposition primarily occur from the NPs that reach the cathode, while they do not occur directly from NP clusters dispersed in the bath. Furthermore, NPs at grain boundaries can inhibit grain growth, preventing columnar grain structures and promoting finer, equiaxed grains. However, at the moment there is no further evidence of this phenomenon other than the results of improved Vickers microhardness measured on the nanocomposite coatings. As a consequence, we wanted to analyze this effect via phase-field simulations.

These modelling assumptions are grounded in experimental studies performed at laboratory and pilot scale. Ni-based nanocomposite coatings were synthesized using modified Watts-type electrolytes, where the conventional boric acid buffer (H_3BO_3) is replaced by combinations of organic acids selected via Safe-and-Sustainable-by-Design (SSbD) criteria. Recent work leveraging generative models to identify SSbD-compliant substitutes for boric acid in nickel electroplating provides additional support for the electrolyte design strategy adopted in our experiments.[30] Hull Cell screenings evaluated 14 candidate acids with different pKa values, of which some of them (e.g., citric, succinic, acetic, glutaric, tartaric and oxalic acid) demonstrated stable pH buffering behaviour and suitable electrodeposition performance. These electrolytes contained Ni^{2+} salts, chloride ions for anode activation, and the selected organic acid as the primary buffering component.

To produce nanocomposite coatings, the electrolytes were reinforced with ceramic (Al_2O_3, SiC) and 2D nanoparticles (graphitic materials such as graphene-based platelets), all of which had been pre-functionalized or dispersed using controlled ultrasonication protocols to ensure stability and prevent aggregation. Surfactants were included when necessary to avoid particle agglomeration and to maintain a uniform size distribution. Their use is consistent with the project's SSbD constraints, meaning that substances listed as Substances of Very High Concern (SVHCs) under Registration, Evaluation, Authorisation and Restriction of Chemicals (REACH) regulations[31] were excluded from all formulations. The NP dispersions were continuously monitored with OF2i (Optofluidic Force Induction),[32,33] DLS, and NTA systems to prevent segregation and to verify absence of particle accumulation at rest, directly supporting our model assumption that NPs remain homogeneously suspended rather than migrating toward the solid–liquid interface.

Furthermore, electrodeposition trials performed at small scale (2 L), bench scale (14 L), and pilot scale (120 L) revealed that nanoparticles do not segregate or accumulate at the cathode surface in the absence of external fields. Instead, they remain in suspension through Brownian motion and hydrodynamic agitation, confirming that their incorporation occurs only upon physical arrival at the cathode during growth. This behaviour was consistently observed across baths containing SiC, Al_2O_3, and 2D materials, aligning with the assumption in our simulations that NP positions are fixed and that no spontaneous clustering takes place during the deposition window.

Finally, the motivation for selecting these specific NP systems originates from experimental friction and wear results showing that Al_2O_3, SiC, and 2D nanomaterials substantially reduce friction coefficients and increase coating durability, particularly under forming or sliding conditions (e.g., friction coefficient mapping and lifetime tests). Their capacity to

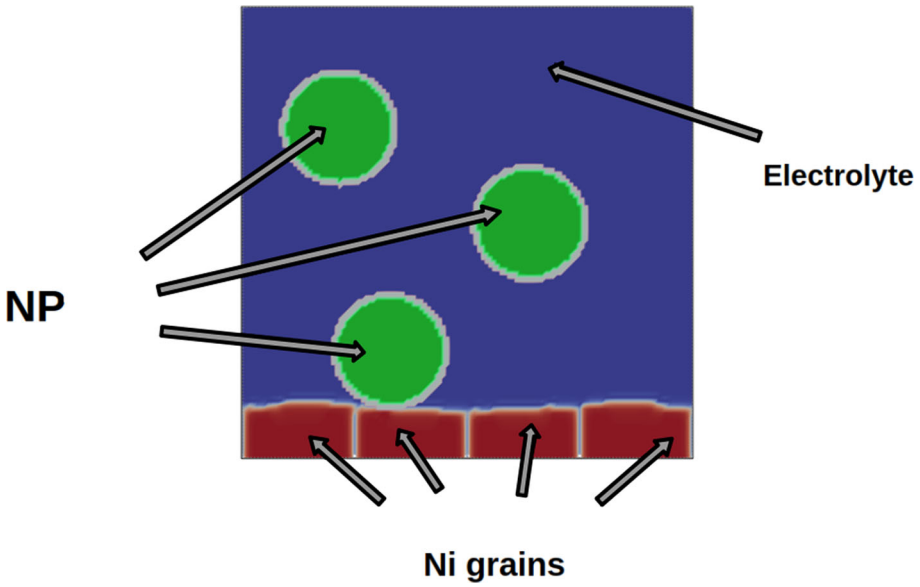

Figure 1. 50 × 50 μm² simulation box containing 4 Ni grains, in red, and three circular NPs, in green. The blue region is occupied by the electrolyte. Periodic boundary conditions apply in the direction perpendicular to grain growth.

modify solidification fronts, through drag reduction (2D materials) or enhanced wettability (metal oxides), makes them ideal candidates for evaluating their influence on columnar growth suppression.

In our computer simulations, the simulation box consisted of a 2-dimensional $50 \times 50\,\mu m^2$ domain containing 5 Ni grains and different number of NPs with same radius as the initial mean grain size (see Figure 1). This setup allowed us to probe the interaction between the growing metal matrix and incorporated particles, and the 2-dimensional approach was enough to reproduce the phenomena. For this, we ran phase-field simulations with circular and rectangular NPs and with different

Table 2. Phase-field model parameters analyzed during this work to study their impact on surface texture.

MODEL VARIABLES			
Symbol	**Meaning**	**Symbol**	**Meaning**
ε	Order parameter representing Ni grains	c	Ion concentration
ϵ	Order parameter representing NPs	ϕ	Electrostatic potential field
CONSTANTS			
Symbol	**Meaning**	**Units**	**Value**
L_σ	Interface mobility	$m^3J^{-1-1}s$	10^{-6}
α	Symmetry number	-	0.5
n	Cation valence	-	2
F	Faraday constant	sA/mol	96485.33
R	Gas constant	J mol^{-1} K^{-1}	8.314
T	Bath Temperature	K	298
σ_e	Electrical conductivity in the electrolyte phase	S/m	1
σ_{Ni}	Electrical conductivity in Ni grains	S/m	10^7
MODEL PARAMETERS			
Symbol	**Meaning**	**Symbol**	**Meaning**
L_η	Mobility-related prefactor	γ_{nuc}	Nucleation Strength by NPs
κ	Gradient Coefficient	γ_{NP}	Effect of NPs on the Ion Diffusion
η	Overpotential	γ^{σ}_{NP}	Effect of NPs on the Conductivity
D	Diffusion Coefficient of Ions	c_s	Site Density
Noise	Thermal Noise	c_0	Ion Concentration in electrolyte

number of NPs. In order to study the impact of process and material parameters on surface roughness and columnar growth, we analyzed the effect of the parameters listed in Table 2 with a random forest classifier,[40] and used xAI with the SHAP tree explainer to understand the impact of the different model parameters individually.

Figure 2 shows the range of values used in 2500 phase-field simulations, with 3 circular NPs and 5 Ni grains.[40] Because these physical parameters span multiple orders of magnitude, sampling was performed logarithmically for kinetic and transport prefactors to ensure uniform coverage across exponential scales. For linear operational controls (such as overpotential), uniform random sampling within physically realistic experimental boundaries was applied. Additionally, simulations with typical values reported in the literature or suggested by experimentalists present in our consortium were also performed. This hybrid sampling scheme explains the discrete binning visible in the histograms. These plots show the number of stable and non-stable simulations, where simulations are classified as stable if they reach the final simulation time while satisfying the convergence criteria of the nonlinear solver at each time step. Conversely, simulations are labeled as unstable when numerical convergence is not achieved and the solver fails to proceed. This classification reflects numerical stability of the solution procedure rather than a physical instability of the electrodeposition process. However, since sensitivity analyses demonstrate that the observed instability is independent of mesh refinement or time-step, we conclude that it is a characteristic of the selected parameter set. Dynamic visualizations of both scenarios are available as supplementary materials (Video S1 for the columnar-growth case and Video S2 for the grain suppression case). Here we can see that, in the first case, the system maintains steady-state columnar growth while the presence of two NPs induces a localized instability that leads to the suppression of one of the columnar grains given a specific choice of model parameters. According to Figure 2, we can see that large overpotential values can lead to unstable simulations, but, regarding the other variables, there is no direct correlation between them individually and the simulation stability. In order to understand the impact of the different variables listed in Table 2 in the stability of the phase-field simulations, we used the SHAP technique with a trained random forest classifier as surrogate model. According to this xAI technique, as we can see in Figure 3, the variables with a larger impact on the simulation stability are the overpotential, as we could deduce from Figure 2 for large absolute values, the mobility prefactor, the site density and the effect of NPs on ion mobility. As we can see in Figure 3, this bee-swarm plot reveals that high absolute values of overpotential and high values of mobility prefactor strongly push predictions toward instability (negative SHAP values), whereas moderate overpotentials promote stability. This analysis underscores that both process conditions (e.g., overpotential) and material properties (e.g., mobility) must be carefully selected for stable and smooth electrodeposition.

For the stable simulations, we also studied the solidification process and distinguished between simulations with columnar and non-columnar grain growth.[40] To distinguish between columnar and non-columnar microstructures, we introduced a quantitative classification criterion based on grain morphology. Columnar growth was identified when at least one of the following conditions was satisfied: one or more grains exhibited negative lateral growth, indicating shrinkage or suppression by neighboring grains; there was a strong disparity in lateral growth between grains, reflected by a large normalized width spread (the difference between the most dominant grain and the most suppressed grain accounts for more than 50% of the total lateral growth); or there was a pronounced anisotropy along the growth direction, indicated by a large normalized height spread, when the difference between the fastest-growing and slowest-growing grains in the growth direction accounts for more than 70% of the total vertical growth. Otherwise, the microstructure is classified as non-columnar. Thus, we observed columnar growth in most simulations, but this behaviour was strongly influenced by the choice of the model parameters. As in the study of the stability of simulations, we used the SHAP technique with a trained random forest classifier as surrogate model to understand the impact of the different variables listed in Table 1 in the type of grain growth during phase-field simulations. As we can see in Figure 4, the gradient coefficient, overpotential, mobility prefactor, site density and nucleation strength are the parameters with a larger impact on columnar growth in the presence of NPs during electrodeposition. Additionally, the bee-swarm plot shows that high values of gradient coefficient (red points) and and small values of overpotential (blue points) shift model predictions toward non-columnar growth (negative SHAP values). This is caused because high gradient energy values penalize interface boundaries and curvature, suppressing column development and driving the microstructure away from columnar growth. While the overpotential is a process parameter that can be set manually, the others are material-dependent, meaning that the choice of the right chemistry is essential to prevent or promote columnar growth. The gradient coefficient parameter and lattice site concentration depend on the chemical specie of the matrix, but the mobility prefactor and nucleation strength can be modified by choosing the right NP type. Therefore, it is important to analyze how the size, concentration, shape and type of NP affects columnar growth.

In order to understand how altering one single parameter in isolation can shift predictions, we generated partial dependence plots (see Figure 5). A partial dependence plot were computed by setting the target feature to a fixed value across all dataset samples, running the trained model on these modified samples and then averaging the predicted outputs to isolate that feature's marginal effect. We observed that the overpotential exhibits a sharp operational transition around -0.30, rising steeply from 0.62 to a peak of 0.88 at milder driving forces. In contrast, the gradient coefficient maintains a

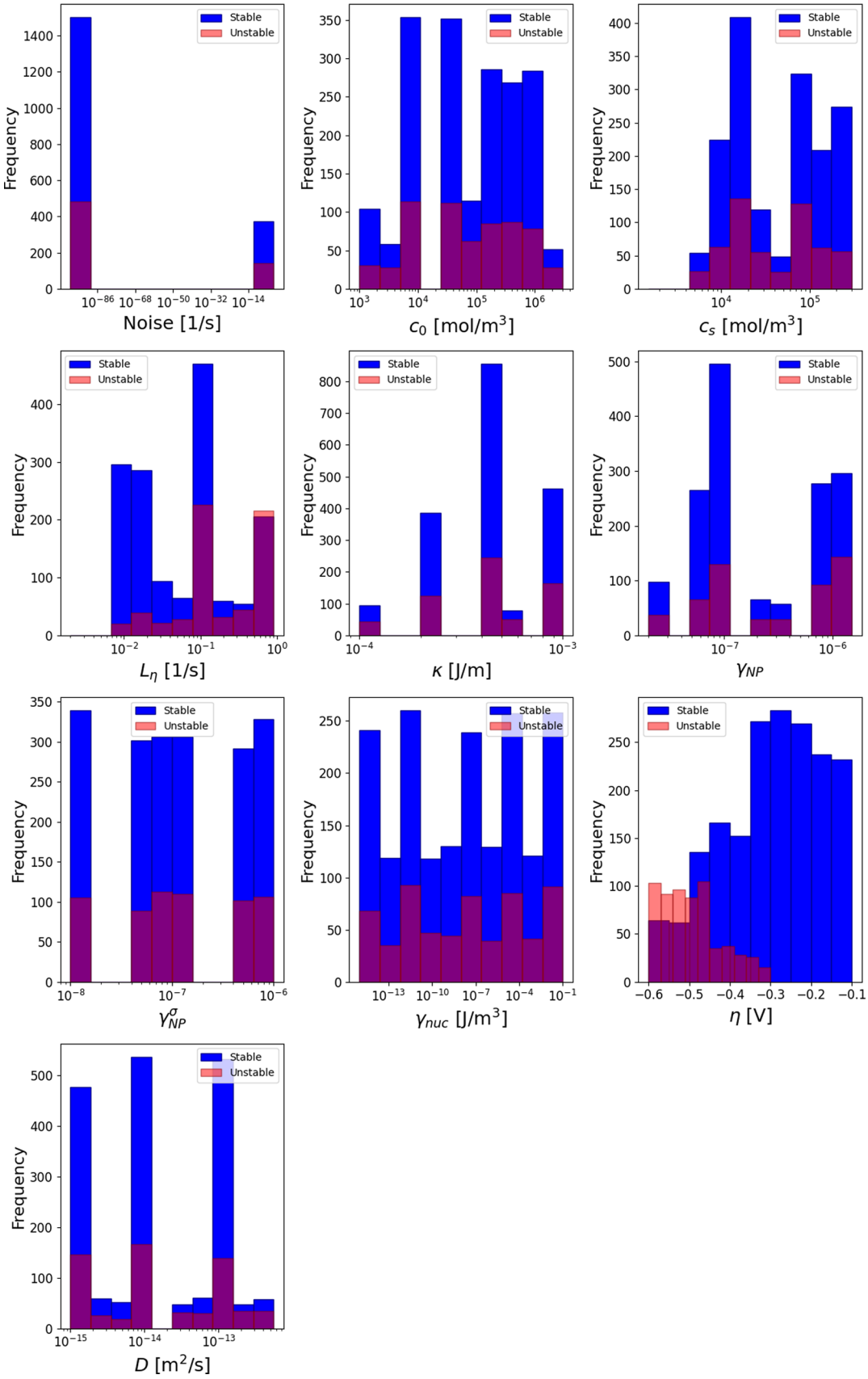

Figure 2. Histograms showing the ranges of values used for the variables listed in Table 1 in phase-field simulations. Simulations were classified into stable or unstable, whether they were completed correctly without crashing or not, respectively.

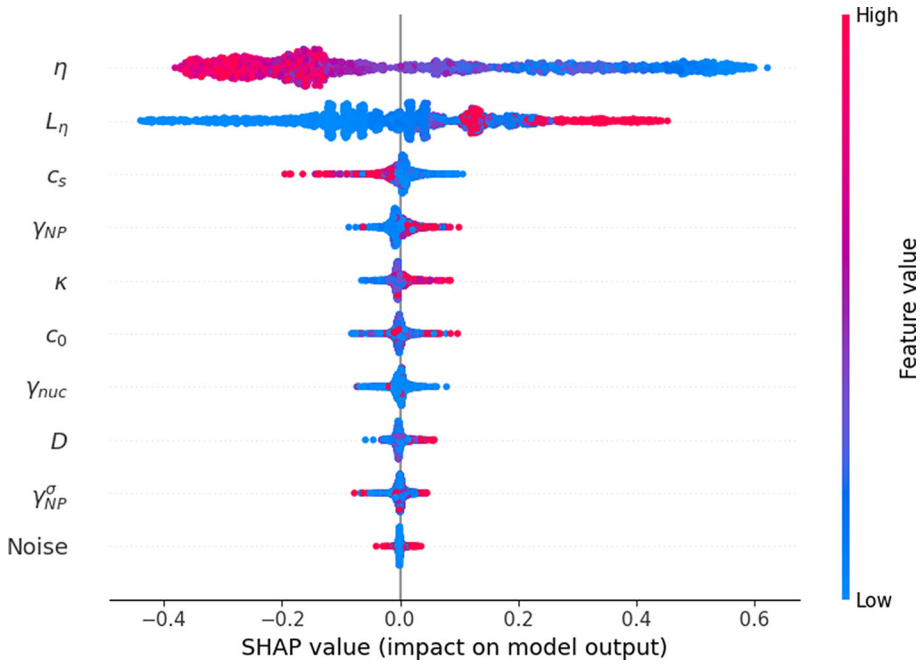

Figure 3. Bee-swarm plot revealing the impact of each model parameter value on the simulation stability, during the classification of simulations into stable or unstable. The model parameters are ranked by their average impact on the output across all simulations. The bar length for each parameter represents the mean absolute SHAP value, a measure of how strongly that parameter influenced the prediction of stable vs unstable simulation, with longer bars indicating greater influence.

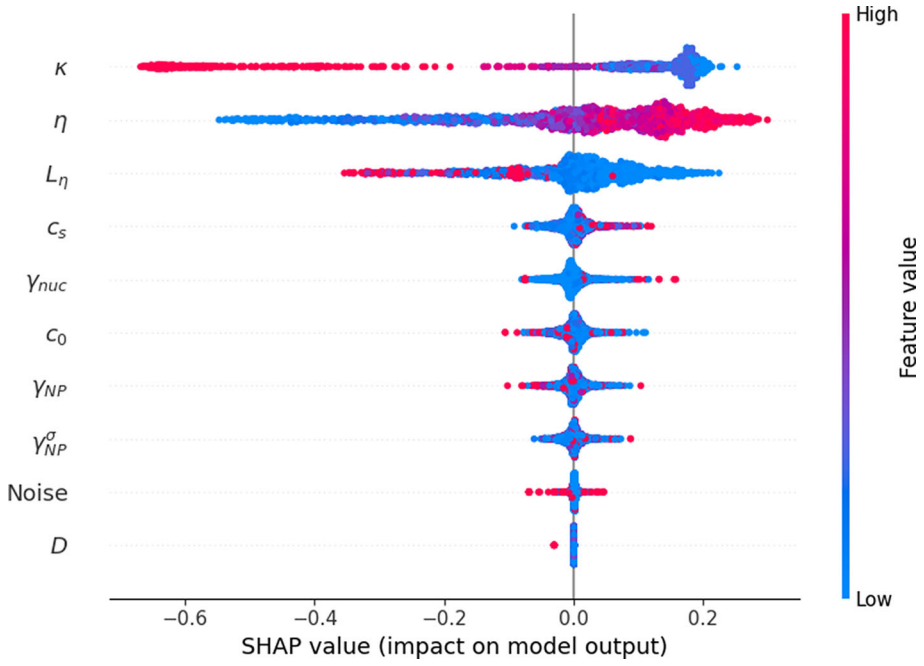

Figure 4. Bee-swarm plot revealing the impact of each simulation parameter value on grain growth, during the classification of grain growth into columnar or non-columnar. The bar length indicates the average SHAP value of each parameter's effect on grain growth. Since the values are sorted, the first features have larger impact on the detection of columnar or non columnar growth.

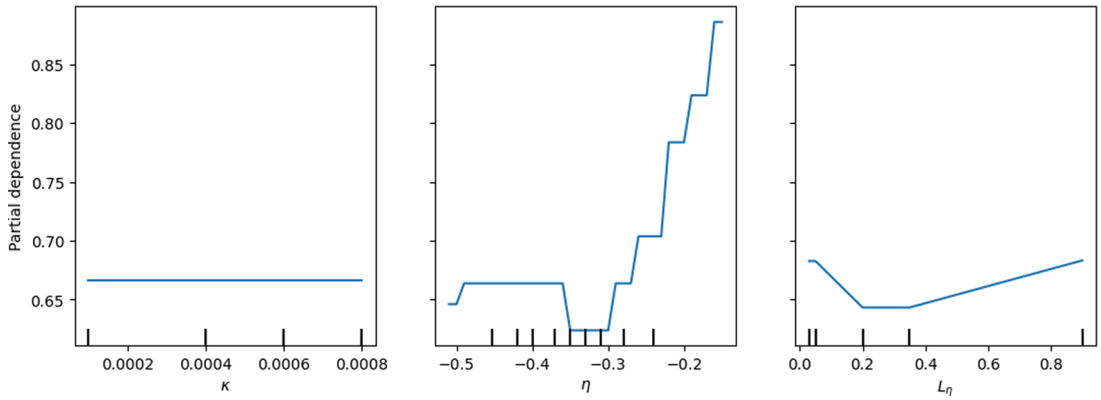

Figure 5. Partial dependence plots illustrating the isolated marginal effects of the gradient energy coefficient, overpotential and interface mobility prefactor on model predictions while holding all other features constant.

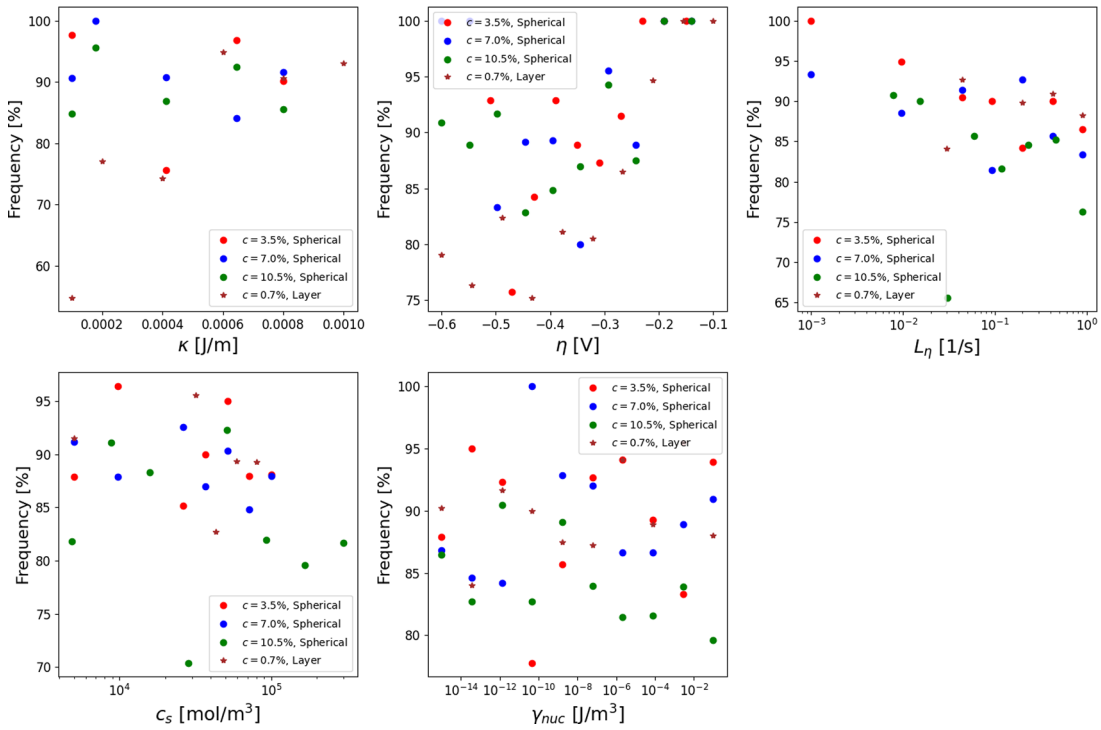

Figure 6. Frequency of simulations in which columnar grain growth was observed, for different NP concentrations and shapes, when varying gradient coefficient, overpotential, mobility prefactor, site density and nucleation strength.

flat response curve, reflecting interaction-dominant behavior, while the mobility prefactor displays a minor non-monotonic dip between 0.20 and 0.35.

Figure 6 shows the frequency of simulations in which columnar grain growth was observed, for different NP volume fractions and sizes as a function of the most relevant input features: varying gradient coefficient, overpotential, mobility prefactor, site density and nucleation strength. In this figure and in Table 3, which provides the associated Pearson correlation coefficient (r) and two-tailed p-value to measure the strength and direction of the relationship between input parameters and frequency of simulations in which columnar growth was observed, we can see that larger mobility prefactor values and higher NP concentrations inhibit columnar growth, as we can see consistently negative Pearson correlation coefficients across all configurations. In general, NPs can reduce impurities or defects at solid-liquid interfaces and often restrict grain growth while indirectly promoting controlled mobility for finer structures. Furthermore,

Table 3. Pearson correlation coefficient (r) and two-tailed p-value for simulations with different NP concentrations and shapes.

Model Parameter	NP shape	NP volume fraction [%]	Pearson correlation coefficient (r)	p-value
κ	Spherical	3.5	−0.082	−0.918
		7.0	−0.498	0.393
		10.5	−0.166	0.789
	Layer	0.7	0.850	0.032
η	Spherical	3.5	0.715	0.020
		7.0	0.092	0.800
		10.5	0.551	0.099
	Layer	0.7	0.871	0.001
L_η	Spherical	3.5	−0.554	0.197
		7.0	−0.521	0.230
		10.5	−0.246	0.556
	Layer	0.7	−0.011	0.986
c_s	Spherical	3.5	−0.195	0.675
		7.0	−0.472	0.285
		10.5	−0.213	0.613
	Layer	0.7	−0.286	0.641
γ_{nuc}	Spherical	3.5	0.298	0.404
		7.0	0.110	0.763
		10.5	−0.466	0.175
	Layer	0.7	−0.184	0.611

hydrophilic NPs enhance wetting and reduce drag at the interface. As a consequence, metal oxides like MgO or Al_2O_3, which enhance interface wettability, and 2D materials like MoS_2 or graphene, which reduce drag and promote smooth interface movement, appear as perfect candidates to control columnar growth during electrodeposition. Additionally, columnar growth is usually less frequent with larger overpotential absolute values and lattice site concentration, in part because the electrodeposition becomes more unstable at large absolute overpotential values. Our results have been validated through experimental data, which confirm that the presence of NPs disrupts the steady-state columnar growth characteristic of traditional Ni plating.[34–37] This suppression of columnar structures in Ni-SiC nanocomposite coatings, a high-performance alternative to conventional chromium electrodeposition, yields significantly higher hardness and wear resistance, demonstrating how ceramic NP integration enhances overall coating characteristics.

The most striking trend is the systematic decrease in columnar growth frequency with increasing NP concentration. At low concentrations (e.g., 1–2 vol%), particles have a marginal effect and they do not inhibit columnar growth efficiently. However, at higher concentrations (e.g., more than 3 vol%), the probability of columnar growth drops. This is a direct demonstration of the Zener pinning effect, where a critical particle density is required to effectively start pinning grain boundaries and slow down their motion. These observations are in good agreement with experimental observations of solidification during additive manufacturing by Narayana Samy et al.,[38] who found that larger particle size and higher volume fraction promoted fine-grained equiaxed structures. Additionally, for a given volume concentration, we observed that 2D NPs consistently outperform spherical ones in suppressing columnar growth. This can be attributed to their larger surface-to-volume ratio, the presence of sharp edges and greater physical footprint, which provides more effective coverage of the grain boundary, creating a stronger drag force.

Additionally, as observed in Figure 6, several model parameters play an important role in the microstructure when they are studied independently. High κ values, associated with high grain boundary energy, inherently resist the curved interfaces of equiaxed structures, favoring columnar growth. However, high NP concentrations can counteract this effect, pinning the boundaries. Similarly, high mobility prefactors (L_η) values, indicating fast interface kinetics, generally promote non-columnar growth by allowing grains to adjust their shape rapidly. With larger values, the electrochemical

reaction occurs faster and very little "overpotential" (driving force) is required to proceed. Then, since the surface is highly active for the reaction, the deposition rate becomes more uniform across the entire surface and growth is not columnar or anisotropic. Additionally, for high overpotentials, the driving force is immense, often leading to non stability and non homogenous growth. Finally, larger nucleation strengths inhibit columnar growth, especially at larger NP concentrations. This parameter accounts for the impact of NPs on liquid/solid/NP interfaces, and is in good agreement with experiments, which highlight that NPs increase the ionic transport on the interface,[39] thus promoting anisotropic growth.

Therefore, this work confirmed that NPs can efficiently control and enhance the properties of electrodeposited coatings. While direct mechanical testing is beyond the scope of this phase-field modeling and ML study, the predicted microstructural structures have clear, well-established implications for the mechanical performance of the electrodeposited coatings. By preventing the formation of columnar grains, which can serve as low-energy pathways for crack propagation and brittle failure, the NP-induced shift toward a non-columnar microstructure fundamentally improves deposit toughness and load-bearing capacity. Thermodynamically and mechanically, the increased grain boundary density resulting from columnar disruption strengthens the Ni matrix. Furthermore, the choice of NP geometry dictates distinct strengthening and wear-reduction modes: discrete spherical ceramic particulates (Al_2O_3, SiC, MgO) are expected to act as pinning sites that exert Zener drag on migrating grain boundaries to enhance microhardness, whereas basal-oriented 2D sheets (MoS_2, graphene) can provide low-shear sliding planes that significantly reduce friction and abrasive wear while preserving structural integrity. The microstructural transitions predicted by our phase-field model in favor of non-columnar regimes directly dictate the macroscopic mechanical performance of electrodeposited Ni composite coatings. While unreinforced electrodeposited pure Ni typically exhibits a coarse columnar microstructure where continuous grain boundaries parallel to the growth direction act as preferential paths for intergranular crack propagation and dislocation motion, when discrete spherical ceramic nanoparticles (Al_2O_3, SiC, MgO) or 2D sheets (MoS_2, graphene) disrupt this directional front, the resulting refinement increases grain boundary area density, which substantially elevates matrix hardness and yield larger strength through Hall–Petch dislocation pile-up and Zener boundary pinning. Furthermore, high-aspect-ratio 2D nanomaterials (MoS_2, graphene) promote smoother growth fronts and isotropic grain interruption at volume fractions above 3%, where the basal-oriented 2D sheets facilitate low-shear sliding contact that dramatically reduces the coefficient of friction in Ni-MoS_2 and Ni-graphene composites. These literature-backed mechanical benchmarks confirm that tuning phase-field parameter windows to prevent columnar growth yields tailored electrodeposits with optimized strength, fracture toughness and wear resistance.

4. Conclusion

In this work, a combined phase-field model and ML approach was used to investigate the role of NPs in controlling the microstructure during nickel electrodeposition. We observed that the stability of the electrodeposition process and the resulting grain morphology (columnar vs. equiaxed) are highly sensitive to key parameters, with the overpotential being the dominant factor for stability, and the gradient coefficient, mobility prefactor and NP characteristics (nucleation strength, concentration and shape) being critical in controlling microstructure. The results indicate that, within the explored parameter space and modelling assumptions, NPs can therefore influence microstructural evolution by modifying interface dynamics and grain growth behavior. The simulations demonstrate that NPs effectively inhibit columnar grain growth by promoting a finer, more equiaxed microstructure. Additionally, with similar concentrations in surface, 2D NPs can produce better results than circular ones, showing that this process is anisotropic and only the direction of the solidification front growth is relevant. Specifically, spherical metal oxides (e.g., MgO, Al_2O_3) enhance wettability and disrupt interface progression, while 2D materials (e.g., MoS_2, graphene) reduce drag and promote smoother solidification fronts, leading to superior surface quality. By preventing the formation of long, straight columnar grain boundaries, which are preferred paths for crack propagation, the NP-induced microstructures predicted by our model are expected to exhibit improved mechanical properties, such as higher toughness and wear resistance. Specifically, we observed that 2D nanomaterials like MoS_2 or graphene are more efficient to prevent columnar growth when their volume fraction is larger than 3%. Therefore, this study based on combined phase-field and ML framework via 2D simulations and SHAP analysis provides insights on the best NP types and concentrations for guiding the design of NP-reinforced electrodeposits. Future work will focus on extending this approach to 3D phase-field modelling to capture more complex topological effects, and on guided experimental validation of the predicted microstructures using the identified optimal parameters (e.g., larger than 3 vol% nanomaterials).

Ethics and consent

Ethical approval and consent were not required.

Data availability

Simulation Results from Phase-Field Study on Electrodeposited Coatings. Registration DOI: https://doi.org/10.5281/zenodo.21902692.[40] This repository contains the simulation data used in this work to train ML algorithms, together with videos representing columnar growth and grain suppression and the codes needed to reproduce the ML techniques used in the present work:

- results_simulations_5g1np_circle.csv: simulation data with varying model variables (first 10 columns, input features) and simulation results (the last 5 columns, targets) obtained with a initial simulation box containing 5 Ni grains and 1 circular NP.
- results_simulations_5g2np_circle.csv: simulation data with varying model variables (first 10 columns, input features) and simulation results (the last 5 columns, targets) obtained with a initial simulation box containing 5 Ni grains and 2 circular NPs.
- results_simulations_5g3np_circle.csv: simulation data with varying model variables (first 10 columns, input features) and simulation results (the last 5 columns, targets) obtained with a initial simulation box containing 5 Ni grains and 3 circular NPs.
- results_simulations_5g3np_rectangle.csv: simulation data with varying model variables (first 10 columns, input features) and simulation results (the last 5 columns, targets) obtained with a initial simulation box containing 5 Ni grains and 3 flat NPs.
- S1.mp4: Video showing an exemple of columnar growth, in the absence of NPs.
- S2.mp4: Video showing an exemple of grain suppression in the presence of circular NPs. The NPs are not shown directly. NPs are present in the circular regions that the grains avoid.
- notebook.ipynb: Jupyter notebook that includes the codes necessary to reproduce the ML techniques used in the work.

Data are available under the terms of the Creative Commons Attribution 4.0 International license.

References

1. Meyers MA, Mishra A, Benson DJ: **Mechanical properties of nanocrystalline materials.** *Prog. Mater. Sci.* 2006; **51**(4): 427–556. Publisher Full Text
2. Sadiku-Agboola O: **The properties and the effect of operating parameters on nickel plating (review).** *International Journal of the Physical Sciences.* 2012; **7**(3). Publisher Full Text
3. Oniciu L, Mureşan L: **Some fundamental aspects of levelling and brightening in metal electrodeposition.** *J. Appl. Electrochem.* 1991; **21**(7): 565–574. Publisher Full Text
4. Shao W, Nabb D, Renevier N, *et al.*: **Mechanical and Anti-Corrosion Properties of TiO_2 Nanoparticle Reinforced Ni Coating by Electrodeposition.** *J. Electrochem. Soc.* 2012; **159**(11): D671–D676. Publisher Full Text
5. Benea L: **Preparation and investigation of nanostructured SiC–nickel layers by electrodeposition.** *Solid State Ionics.* Nov. 2002; **151**(1–4): 89–95. Publisher Full Text
6. Nicoleta B, Lidia B, Daniela-Laura B, *et al.*: **Nanostructuring Effect of Nano-CeO2 Particles Reinforcing Cobalt Matrix during Electrocodeposition Process.** *Nanomaterials.* Aug. 2022; **12**(17): 2923. Publisher Full Text
7. Mohanty US: **Electrodeposition: A versatile and inexpensive tool for the synthesis of nanoparticles, nanorods, nanowires, and nanoclusters of metals.** *J. Appl. Electrochem.* Mar. 2011; **41**(3): 257–270. Publisher Full Text
8. Batista JNM, *et al.*: **Controlling silicate meso-structures using sucupira oil as a new swelling agent.** *Appl. Surf. Sci.* Apr. 2012; **258**(12): 5111–5116. Publisher Full Text
9. Torabinejad V, Rouhaghdam AS, Aliofkhazraei M, *et al.*: **Electrodeposition of Ni–Fe and Ni–Fe-(nano Al 2 O 3) multilayer coatings.** *J. Alloys Compd.* Feb. 2016; **657**: 526–536. Publisher Full Text
10. Liu J, Liu C, Conway PP: **Kinetic Monte Carlo simulation of electrodeposition of polycrystalline Cu.** *Electrochem. Commun.* Nov. 2009; **11**(11): 2207–2211. Publisher Full Text
11. Zargarnezhad H, Dolati A: **A 3D Continuum-Kinetic Monte Carlo Simulation Study of Early Stages of Nucleation and Growth in Ni Electrodeposition.** *Electrochim. Acta.* May 2017; **236**: 1–9. Publisher Full Text
12. Mamme MH, *et al.*: **A Finite Element Simulation of the Electrochemical Growth of a Single Hemispherical Silver Nucleus.** *Electrochim. Acta.* Apr. 2016; **197**: 307–317. Publisher Full Text
13. Brant AM, Sundaram M: **A Fundamental Study of Nano Electrodeposition Using a Combined Molecular Dynamics and Quantum Mechanical Electron Force Field Approach.** *Procedia Manuf.* 2017; **10**: 253–264. Publisher Full Text
14. Steinbach I: **Phase-field models in materials science.** *Model. Simul. Mater. Sci. Eng.* 2009; **17**(7): 073001. Publisher Full Text

15. Shibuta Y, Okajima Y, Suzuki T: **Phase-field modeling for electrodeposition process.** *Sci. Technol. Adv. Mater.* Jan. 2007; **8**(6): 511–518.
Publisher Full Text

16. Li J, Zheng D, Zhang W: **Advances of Phase-Field Model in the Numerical Simulation of Multiphase Flows: A Review.** *Atmos.* Aug. 2023; **14**(8): 1311.
Publisher Full Text

17. Chen L-Q: **Phase-Field Models for Microstructure Evolution.** *Annu. Rev. Mater. Res.* Aug. 2002; **32**(1): 113–140.
Publisher Full Text

18. Liu Z, *et al.*: **Dendrite-free Lithium Based on Lessons Learned from Lithium and Magnesium Electrodeposition Morphology Simulations.** *Cell Rep. Phys. Sci.* Jan. 2021; **2**(1): 100294.
Publisher Full Text

19. Guan T, Zhang N: **Recent Advances in Electrodeposition of Nickel-Based Nanocomposites Enhanced with Lubricating Nanoparticles.** *Nanomanufacturing and Metrology.* Dec. 2024; **7**(1): 25.
PubMed Abstract | Publisher Full Text | Free Full Text

20. Lee SH, Woo SP, Kakati N, *et al.*: **A Comprehensive Review of Nanomaterials Developed Using Electrophoresis Process for High-Efficiency Energy Conversion and Storage Systems.** *Energies.* Nov. 2018; **11**(11): 3122.
Publisher Full Text

21. Farade RA, Abdul Wahab NI, Rafiq M, *et al.*: **Cutting-edge dielectric nanofluids: A review of factors influencing stability and thermo-dielectric properties.** *J. Therm. Anal. Calorim.* Nov. 2025; **150**(23): 18917–18965.
Publisher Full Text

22. Logg A, Mardal K-A, Wells G: **Automated Solution of Differential Equations by the Finite Element Method.** *The FEniCS Book.* Springer; 1st ed. 2012.

23. Aln MS, *et al.*: **The FEniCS Project Version 1.5.** *Archive of Numerical Software.* 2015; **3**(100): 9–23.

24. More AS, Rana DP: **Review of random forest classification techniques to resolve data imbalance.** *2017 1st International Conference on Intelligent Systems and Information Management (ICISIM).* Aurangabad: IEEE; Oct. 2017; 72–78.
Publisher Full Text

25. Lundberg SM, *et al.*: **From local explanations to global understanding with explainable AI for trees.** *Nature Machine Intelligence.* Jan. 2020; **2**(1): 56–67.
PubMed Abstract | Publisher Full Text | Free Full Text

26. Lundberg S, Lee S-I: **A Unified Approach to Interpreting Model Predictions.** *arXiv.* Nov. 2017.
Publisher Full Text

27. Bełtowska-Lehman E, Góral A, Indyka P: **Electrodeposition and Characterization of Ni/Al2O3 Nanocomposite Coatings.** *Arch. Metall. Mater.* Jan. 2011; **56**(4).
Publisher Full Text

28. Pinate S, Ispas A, Leisner P, *et al.*: **Electrocodeposition of Ni composites and surface treatment of SiC nano-particles.** *Surf. Coat. Technol.* Jan. 2021; **406**: 126663.
Publisher Full Text

29. Kamel MM, Hamid ZA, Rashwan SM, *et al.*: **Electrodeposition of Ni–Co/nano Al2O3 composite coating on low carbon steel and its characterization.** *Int. J. Electrochem. Sci.* Jul. 2020; **15**(7): 6343–6358.
Publisher Full Text

30. Coto AG, Precker CE, RodrıgUez LH, *et al.*: **Generative and evolutionary approaches for safe and sustainable by design material development: A case study on acid alternatives for advanced material coatings.** *2025 11th international conference on computing and artificial intelligence (ICCAI).* 2025; 736–745.
Publisher Full Text

31. REACH regulations:**7**: 25.
PubMed Abstract | Free Full Text | Reference Source

32. Šimić M, Neuper C, Hohenester U, *et al.*: **Optofluidic force induction as a process analytical technology.** *Anal. Bioanal. Chem.* Sep. 2023; **415**(21): 5181–5191.
PubMed Abstract | Publisher Full Text | Free Full Text

33. Šimić M, Neuper C, Hauer R, *et al.*: **Optofluidic Force Induction: A Workbench for Nanoparticle Characterization and Material Analytics.** *Nano Lett.* Jun. 2025; **25**(22): 8805–8813.
PubMed Abstract | Publisher Full Text | Free Full Text

34. Chakraborty S, *et al.*: **Are Ni–SiC nanoparticle electroplated coatings a safer alternative to hard chromium? A comprehensive aging, toxicity, and in Silico study to assess safety by design.** *Environ. Sci. Nano.* 2025; **12**(1): 894–908.
Publisher Full Text

35. Dhakne A, Jaju S, Shukla S: **A review on wear characterization of electrodeposited nickel matrix composites.** *IOP Conference Series: Materials Science and Engineering.* Oct. 2022; **1259**(1): 012050.
Publisher Full Text

36. Guan T, Zhang N: **Recent Advances in Electrodeposition of Nickel-Based Nanocomposites Enhanced with Lubricating Nanoparticles.** *Nanomanufacturing and Metrology.* Dec. 2024; **7**(1): 25.
PubMed Abstract | Publisher Full Text | Free Full Text

37. Hamoudi S, Bezzi N, Bensebaa F, *et al.*: **Alumina–Nano-Nickel Composite Coatings on Al6061 Substrate Obtained by Electrophoretic Deposition.** *J. Compos. Sci.* Mar. 2025; **9**(3): 122.
Publisher Full Text

38. Narayana Samy VP, Schäfle M, Brasche F, *et al.*: **Understanding the mechanism of columnar–to-equiaxed transition and grain refinement in additively manufactured steel during laser powder bed fusion.** *Addit. Manuf.* 2023; **73**: 103702.
Publisher Full Text

39. Benea L, *et al.*: **Composite Electrodeposition to Obtain Nanostructured Coatings.** *J. Electrochem. Soc.* 2001; **148**(7): C461.
Publisher Full Text

40. Troncoso JF: Simulation Results from Phase-Field Study on Electrodeposited Coatings. [Dataset]. *Zenodo.* 2026.
Publisher Full Text

Open Peer Review

Current Peer Review Status: ? ?

Version 1

Reviewer Report 30 September 2026

https://doi.org/10.21956/openreseurope.26761.r81401

© **2026 Velayudham S.** This is an open access peer review report distributed under the terms of the Creative Commons Attribution License, which permits unrestricted use, distribution, and reproduction in any medium, provided the original work is properly cited.

?

Suresh Velayudham
[1] Sona College of Technology, Salem, Tamil Nadu, India
[2] Sona College of Technology, Salem, Tamil Nadu, India

After going through the manuscript, the following issues are suggested to consider for the improvement of the manuscript.

1. The chemical formula should be consistently written as MoS_2 throughout the manuscript.
2. While the abstract refers to 2D materials like graphene and MoS_2, the introduction lacks any background on these materials or justification for their selection. Please include a discussion of graphene and MoS_2 in the introduction, along with the reasoning behind choosing these specific materials for the study.
3. Figure 1: The direction of the arrows has been reversed to improve clarity and make the figure easier for readers to understand.
4. In the Results and Discussion section, the authors have mentioned Al_2O_3 and other particles/materials such as MgO and SiC. However, these materials are not introduced in the Abstract or Introduction, and they are also not represented in Figure 1. Furthermore, the manuscript does not provide sufficient experimental data or detailed discussion regarding the performance and role of these materials. The authors are requested to ensure consistency throughout the manuscript and provide adequate supporting data and discussion for all the materials considered.
5. The study primarily employs the Random Forest Classifier and SHAP Tree Explainer. However, several other machine-learning and artificial-intelligence algorithms are available for similar prediction and classification tasks. The authors should consider comparing the obtained results with those from other appropriate AI/ML algorithms to demonstrate the effectiveness and reliability of the proposed approach. The reasons for selecting Random Forest should also be clearly justified.
6. The manuscript does not provide sufficient data related to mechanical characterization. Since mechanical properties are important for evaluating the performance and applicability of the investigated material/system, the authors should include relevant mechanical characterization results, along with appropriate analysis and discussion.

Overall, the manuscript addresses a relevant and interesting topic. However, several issues need to be addressed, particularly regarding the consistency of the materials discussed, the justification and comparison of the AI/ML methods employed, and the inclusion of adequate mechanical characterization data. Therefore, the manuscript can be considered for acceptance subject to major revision after the authors satisfactorily address the above comments.

Is the work clearly and accurately presented and does it cite the current literature?
No

Is the study design appropriate and does the work have academic merit?
Partly

Are sufficient details of methods and analysis provided to allow replication by others?
Yes

If applicable, is the statistical analysis and its interpretation appropriate?
Partly

Are all the source data underlying the results available to ensure full reproducibility?
Yes

Are the conclusions drawn adequately supported by the results?
Yes

Competing Interests: No competing interests were disclosed.

Reviewer Expertise: Nano coatings and ML

I confirm that I have read this submission and believe that I have an appropriate level of expertise to confirm that it is of an acceptable scientific standard, however I have significant reservations, as outlined above.

Author Response 05 Oct 2026

Javier Fernández Troncoso

1. The chemical formula should be consistently written as MoS_2 throughout the manuscript.

Response: Corrected in the updated version of the manuscript.

1. While the abstract refers to 2D materials like graphene and MoS_2, the introduction lacks any background on these materials or justification for their selection. Please include a discussion of graphene and MoS_2 in the introduction, along with the reasoning behind choosing these specific materials for the study.

Response: In the revised version of the manuscript, we have updated the Introduction section to introduce the importance of these nanomaterials, and how they can suppress columnar growth.

1. Figure 1: The direction of the arrows has been reversed to improve clarity and make

the figure easier for readers to understand.

Response: Figure 1 has been updated in the revised version of the manuscript.

1. In the Results and Discussion section, the authors have mentioned Al_2O_3 and other particles/materials such as MgO and SiC. However, these materials are not introduced in the Abstract or Introduction, and they are also not represented in Figure 1. Furthermore, the manuscript does not provide sufficient experimental data or detailed discussion regarding the performance and role of these materials. The authors are requested to ensure consistency throughout the manuscript and provide adequate supporting data and discussion for all the materials considered.

Response: In the revised version of the manuscript, we have updated the Introduction section to introduce the importance of these nanomaterials, and how they can suppress columnar growth.

1. The study primarily employs the Random Forest Classifier and SHAP Tree Explainer. However, several other machine-learning and artificial-intelligence algorithms are available for similar prediction and classification tasks. The authors should consider comparing the obtained results with those from other appropriate AI/ML algorithms to demonstrate the effectiveness and reliability of the proposed approach. The reasons for selecting Random Forest should also be clearly justified.

Response: We added a comparative benchmark study in Section 3 evaluating Random Forest (RF), XGBoost, Support Vector Machine (SVM with RBF kernel), k-Nearest Neighbors (k-NN), and Multi-Layer Perceptron (MLP) and justify the use of RFs in the study. We observed that the random forest was the model that maximizes the precision for the prediction of unstable simulations,

1. The manuscript does not provide sufficient data related to mechanical characterization. Since mechanical properties are important for evaluating the performance and applicability of the investigated material/system, the authors should include relevant mechanical characterization results, along with appropriate analysis and discussion.

Response: We have added a new paragraph at the end of the Results&Discussion Section to address this comment.

Competing Interests: No competing interests were disclosed.

Reviewer Report 24 September 2026

https://doi.org/10.21956/openreseurope.26761.r80632

© 2026 Pence M. This is an open access peer review report distributed under the terms of the Creative Commons Attribution License, which permits unrestricted use, distribution, and reproduction in any medium, provided the original work is properly cited.

?

Michael A Pence
[1] The University of Utah, Salt Lake City, Utah, USA
[2] The University of Utah, Salt Lake City, Utah, USA

The work by Troncoso et al. presents a combined simulation and ML study of electrodeposition in the presence of nanoparticle additives. They used phase field modelling to generate a large number of electrodepositions simulations and then used ML to better understand the relationship between input simulation parameters and the resulting convergence and outcomes of the simulations. The paper was informative and useful but has some issues that must be addressed before it can be approved.

In regard to the form, the following brief explanations are provided with more specific suggestions and comments below.
-The work could be better presented, particularly by improving the information presented in the figures.
-The study designed could be improved by better exploring and optimizing different ML models.
-The work does not provide the code used for the simulation or the machine learning code. This greatly limits replication and must be addressed.
-The statistical analysis is partly appropriate, but many decisions are arbitrary and need to be better justified, ie, model selection and choice of parameter values.
-The source data is only partly enough. The authors provide results of simulations but no underlying code for simulations or ML modelling.

More specifically the following comments should be addressed before article approval.
1. Controls based upon the results of the interpretable machine learning analysis would be useful. For the most important parameters, if the other parameters are held constant, what is the behavior on the output. Is there a specific range of these important values that leads to stable/unstable or columnar/non-columnar results?
2. I cannot access the videos showcasing the differences in growth. Regardless, it would be helpful for readers if this was included in the manuscript so they can easily picture what the different outcomes look like.
3. Could the authors elaborate on how they sampled the parameter space for their simulation data? The distributions of values shown in Figure 2 seem to be sampled in an arbitrary manner.
4. There is no explanation behind the chosen hyper-parameters for the Random Forest model. Typically, one would perform cross-validation to tune the hyper-parameter for a model, before determining the model's performance on the test set. Could the authors perform cross-validation studies?
5. Could the authors explain why Random Forest was specifically used as opposed to other comparable ML models (SVM, kNN, gradient boosted trees)? How do other models (with tuned hyper parameters) perform compared to Random Forest?
6. Showing bee swarm plots for the SHAP analysis in Figures 3 and 4 would help interpretation. It is unclear from just a mean SHAP value how the relationship between parameter values and the simulation results (ie does a high/low parameter value make the simulation more/less stable).
7. Figure 5 would be more beneficial if it contained metrics to evaluate correlation between the different parameters and frequency of columnar growth. Even just having trendlines and Pearson correlation coefficients would be helpful to visualize the impact of the different parameters.
8. I do not see links to access the code used to generate simulated data, or the reproduction of the machine learning results. Both should be included in the manuscript.

Is the work clearly and accurately presented and does it cite the current literature?

Partly

Is the study design appropriate and does the work have academic merit?
Partly

Are sufficient details of methods and analysis provided to allow replication by others?
No

If applicable, is the statistical analysis and its interpretation appropriate?
Partly

Are all the source data underlying the results available to ensure full reproducibility?
Partly

Are the conclusions drawn adequately supported by the results?
Yes

Competing Interests: No competing interests were disclosed.

Reviewer Expertise: I have expertise in electrochemistry, lab automation, and machine learning.

I confirm that I have read this submission and believe that I have an appropriate level of expertise to confirm that it is of an acceptable scientific standard, however I have significant reservations, as outlined above.

Author Response 05 Oct 2026

Javier Fernández Troncoso

1. Controls based upon the results of the interpretable machine learning analysis would be useful. For the most important parameters, if the other parameters are held constant, what is the behavior on the output. Is there a specific range of these important values that leads to stable/unstable or columnar/non-columnar results?
Response: We have incorporated these Partial Dependence Plots into Section 3 (Figure 5) of the revised manuscript to clearly delineate parameter thresholds and isolated model behaviors, and have included the interpretation in the revised version of the manuscript.

2. I cannot access the videos showcasing the differences in growth. Regardless, it would be helpful for readers if this was included in the manuscript so they can easily picture what the different outcomes look like.
Response: These videos are also available on the Zenodo repository now and as supplementary material.

3. Could the authors elaborate on how they sampled the parameter space for their simulation data? The distributions of values shown in Figure 2 seem to be sampled in an arbitrary manner.
Response: We updated Section 3 to clarify the sampling strategy. Because the physical

parameters in electrodeposition models span multiple orders of magnitude (e.g., L_η, D, κ, γ_{nuc}), sampling was performed logarithmically for kinetic and transport prefactors to ensure uniform coverage across exponential scales (log10 space). For linear operational controls (such as overpotential η), uniform random sampling within physically realistic experimental boundaries was applied. Additionally, simulations with typical values reported in the literature or suggested by experimentalists present in our consortium were also performed. This hybrid sampling scheme explains the discrete binning visible in the Figure 2 histograms.

4. There is no explanation behind the chosen hyper-parameters for the Random Forest model. Typically, one would perform cross-validation to tune the hyper-parameter for a model, before determining the model's performance on the test set. Could the authors perform cross-validation studies?
Response: We conducted a systematic hyperparameter grid search evaluation to tune the key Random Forest parameters: the number of estimators and the maximum tree depth (max_depth). Specifically, we evaluated candidate model configurations evaluating across numbers of estimators from 25 to 475 in increments of 25 and depth bounds including unconstrained depth (None) and depths from 1 to 46 in steps of 5. We included this text in Section 2.b of the manuscript.

5. Could the authors explain why Random Forest was specifically used as opposed to other comparable ML models (SVM, kNN, gradient boosted trees)? How do other models (with tuned hyper parameters) perform compared to Random Forest?
Response: We added a comparative benchmark study in Section 3 evaluating Random Forest (RF), XGBoost, Support Vector Machine (SVM with RBF kernel), k-Nearest Neighbors (k-NN), and Multi-Layer Perceptron (MLP) and justify the use of RFs in the study. We observed that the random forest was the model that maximizes the precision for the prediction of unstable simulations.

6. Showing bee swarm plots for the SHAP analysis in Figures 3 and 4 would help interpretation. It is unclear from just a mean SHAP value how the relationship between parameter values and the simulation results (ie does a high/low parameter value make the simulation more/less stable).
Response: Figures 3 and 4 have been replaced to include bee-swarm plots. The conclusions are also described in the manuscript (Section 3):

- Figure 3 (Stability): The bee-swarm plot reveals that high absolute values of overpotential and high values of mobility strongly push predictions toward instability (negative SHAP values), whereas moderate overpotentials promote stability.
- Figure 4 (Grain Growth): The bee-swarm plot shows that high values of gradient coefficient (red points) and small values of overpotential (blue points) shift model predictions toward non-columnar growth (negative SHAP values). This is caused because high gradient energy values penalize interface boundaries and curvature, suppressing column development and driving the microstructure away from columnar growth.

7. Figure 5 would be more beneficial if it contained metrics to evaluate correlation between the different parameters and frequency of columnar growth. Even just having trendlines

and Pearson correlation coefficients would be helpful to visualize the impact of the different parameters.
Response: We have added Table 3 with Pearson coefficient correlations and p-values to compare the different images and conclusions drawn from them.

8. I do not see links to access the code used to generate simulated data, or the reproduction of the machine learning results. Both should be included in the manuscript.
Response: We added the jupyter notebook on Zenodo to replicate machine learning analysis. The Fenics codes used to run the Phase-Field model have not been submitted, since they are to be kept as commercial secret. However, since all equations are listed, the model shown in the manuscript is completely reproducible and replicable.

Competing Interests: No competing interests were disclosed.